Chapter 1

Overview

Is the azure of the sky its true color? Or is it that the distance into which we are looking is infinite? The P'eng never stops flying higher till everything below looks the same as above: heat-hazes, dust-storms, the breath which living things blow at each other ...

–Chuang-tzu, 1

1.1 Cosmological Background

With the discovery of the cosmic microwave background (CMB) by Penzias and Wilson in 1965 [128], modern cosmology was born. Long the realm of armchair philosophers, the study of the origins and evolution of the universe became a physical science with falsifiable theories. As light from an earlier epoch, the CMB provides evidence that has proven many a cosmological theory wrong. Still, cosmology has remained a data-starved field until quite recently. Unlike its brethren disciplines, experimentation is not possible. Given access to this one universe alone, one must piece together the principles of its formation out of what observations of it are possible. The task is made even more challenging due to the enormous range of physical and temporal scales involved.

We are now at the threshold of a new era in cosmology. With telescopes probing ever earlier epochs and larger volumes, we are making rapid progress in improving the quantity and quality of data. Cosmology is at last becoming a precision science. Once again the CMB is taking a central place in this transition. Launched in late 1989, the *COBE* satellite ushered in the era of precision cosmology. It has revealed in the CMB a perfect thermal or blackbody spectrum of temperature $T_0 = 2.726 \pm 0.010\mathrm{K}$ (95% CL), with

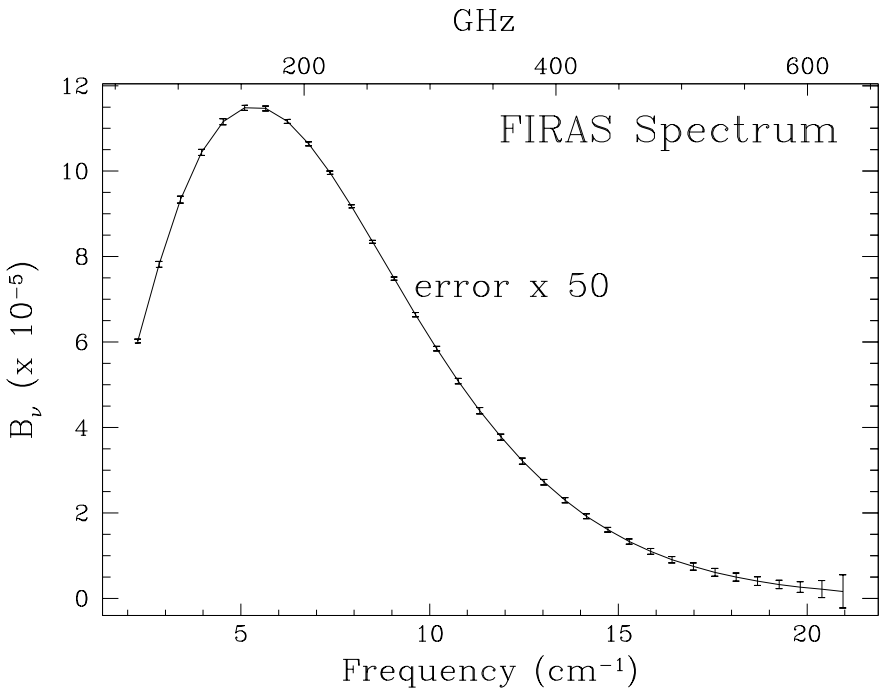

Figure 1.1: FIRAS Spectral Measurement

To the precision of the *COBE* FIRAS instrument [116], the CMB spectrum is a perfect blackbody with a maximum deviation of no more than 3×10^{-4} and a noise weighted rms deviation of under 5×10^{-5} of its peak intensity. No spectral distortions have been measured to date excluding nearly all options for its formation except in the early stages of a hot big bang. Plotted here is the intensity in ergs cm^{-2} s^{-1} sr^{-1} cm.

deviations no more than several parts in 10^4 [116], and temperature anisotropies at the level of one part in 10^5 [153].

1.1.1 Perfection and Its Implications

Observe the void – its emptiness emits a pure light.
–Chuang-tzu, 4

The cosmic microwave background spectrum and anisotropy: near perfection and slight imperfection. The implications of the former run deep; the applications of the latter are broad. A thermal radiation background is a definite and almost unique prediction of the big bang cosmology. Why is the spectrum thermal at 2.7K, a much lower temperature than most astronomical matter in the universe? Let us recall the basic facts and premises upon which the big bang model is built. Light from distant galaxies is redshifted in proportion to

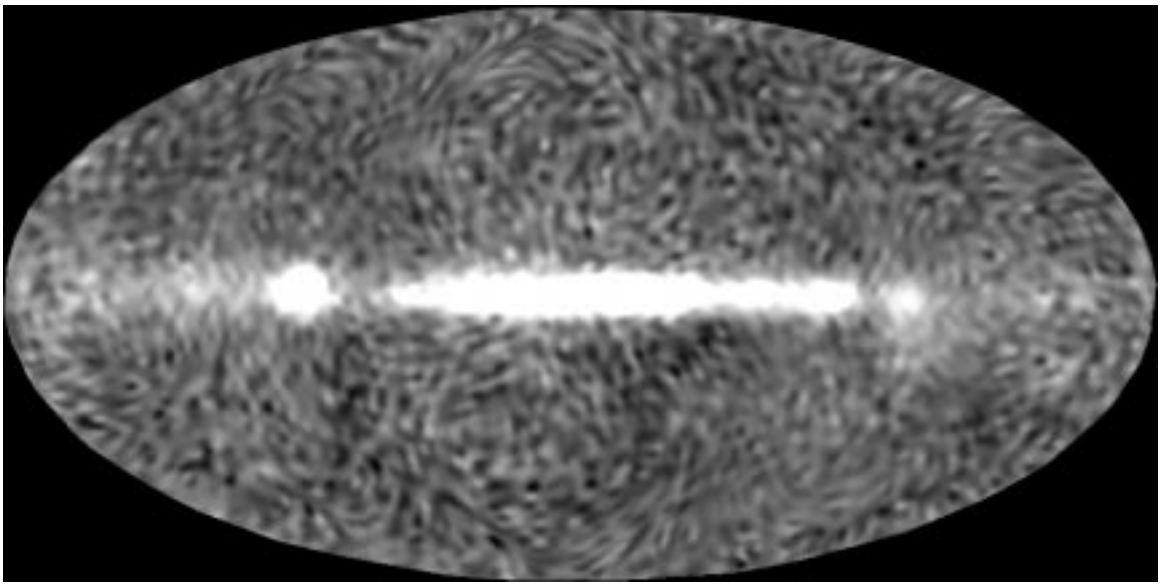

Figure 1.2: DMR Anisotropy Map

Anisotropies in the CMB as detected by the *COBE* DMR experiment at an rms level of $\Delta T/T = \mathcal{O}(10^{-5})$. While the raw data set is noisy and suffers galactic contamination (bright center band), filtering reveals a detection of high significance and importance to our understanding of structure formation in the universe. Map courtesy of E. Bunn.

their distance. In the big bang model, this is interpreted as a consequence of the universal expansion of the universe. Due to the light travel time, distant sources emitted their light long ago when the universe was smaller. During the expansion, the wavelengths of photons are stretched and particle number densities drop leading to the low temperature and photon density observed in the background today. Conversely, extrapolating backwards in time, we infer that the universe began in a hot dense state. As we discuss in more detail in §3, at sufficiently high temperatures interactions between particles were rapid enough to bring the universe into a state of thermal equilibrium. This and the fact that adiabatic cooling from the expansion preserves the thermal spectrum explains the blackbody nature of the observed spectrum (see Fig. 1.1). No other model for cosmology yet proposed can account for the stunningly thermal spectrum. Even in the big bang model, the lack of distortions to the spectrum provides serious constraints on physical and astrophysical processes that could have occurred between the thermalization redshift $z \simeq 10^7$ and the present, *i.e.* very nearly the *whole* history of the universe.

The second pillar upon which the big bang model stands is the large scale homogeneity and isotropy of the universe. Originally only a hypothesis based on simplicity and a Copernican desire not to occupy a preferred position in the universe, this "cosmological principle" finds its validation most dramatically in the radio source catalogue of Gregory and Condon [66] and in the extreme isotropy of the CMB. Aside from a dipole anisotropy of 3.343 ± 0.016mK (95% CL) [152], almost certainly due to the Doppler effect from our own motion, the CMB is isotropic at the level of one part in 10^5.

In fact, the high degree of isotropy has long been a puzzle to cosmologists. The CMB last interacted with the matter through Compton scattering as long ago as redshift $z \simeq 10^3$, when the photons no longer had the energy to keep hydrogen photoionized, and no later than z of a few tens if hydrogen was ionized by some external source. Our extrapolation backwards to this early time tells us that the patches of sky off which the CMB last scattered should not have been in causal contact at that time. This seemingly acausal isotropy of the CMB temperature is called the *horizon problem*. The most promising solution to date, called the inflationary scenario, postulates an early phase of rapid expansion that separates originally causally connected regions by the vast distances necessary to account for the large scale isotropy of the CMB. Alternatively, it may be just a boundary condition of the universe imposed by unknown physics at the Planck epoch.

Potentially more troubling to cosmologists is the fact that the universe at small scales is manifestly inhomogeneous as the distribution of galaxies and indeed our own existence implies. In the big bang model, perturbations grow by gravitational instability slowly due to the expansion, *i.e.* power law rather than exponential growth (see §4, §5). Even though the CMB bears the imprint of an earlier and less evolved epoch, fluctuations must be present at the $10^{-6} - 10^{-5}$ level to be consistent with the simple gravitational instability model. The announcement by the *COBE* DMR group of the first detection of CMB anisotropies was thus met with expressions of relief and elation by cosmologists.

1.1.2 Imperfection and Its Applications

Said Hui-Shih to Chuang-tzu: 'This talk of yours is big but useless.'
–Chuang-tzu, 1

As is often the case in physics, the deviations are of greater practical interest than the mean. While measurements of the thermal nature and isotropy of the CMB reveal strong support for the general hot big bang scenario, they are shed no light upon the details of

the cosmological model. Anisotropies on the other hand bear the imprint, filtered through the dynamics and geometry of the expanding universe, of the fluctuations which eventually led to structure formation in the universe. CMB anisotropies can therefore shed light on not only the mysteries of structure formation but also such fundamental quantities as the expansion rate, matter content and geometry of the universe. Let us briefly review the current status of some of these unresolved issues.

Hubble's law states that the observed redshift scales with distance as $z = H_0 d$ due to the uniform expansion. Measurement of the proportionality constant, the so-called Hubble constant, is notoriously difficult due to the need to obtain absolute distances to galaxies. The uncertainty is usually parameterized as $H_0 = 100h$ km s^{-1} Mpc^{-1} where observations roughly require $0.5 \gtrsim h \gtrsim 1$. High values of the Hubble constant $h \simeq 0.8$ seem currently favored by many distance scale calibrations (see [89] for a review and [56] for recent advances), but the issue is far from settled (see *e.g.* [139]). Because H_0 sets the expansion time scale $H_0^{-1} \simeq 10h^{-1}$Gyr, its measurement is crucial in determining the age of the universe. Through the theory of stellar evolution, globular clusters are inferred to be as old as 14 ± 2 Gyr [140, 141] which may lead to an age crisis if H_0 turns out to be in the upper range of modern measurements.

How acute the age crisis might be depends on the second major source of dispute: the density of the universe. Because mass tends to deccelerate the expansion, a higher energy density implies a younger universe. The mass is usually parameterized by Ω_0 which is the energy density in units of the critical density $\rho_{crit} = 3H_0^2/8\pi G = 1.879 \times 10^{-29} h^2$ g cm^{-3}. There is also the possibility that vacuum energy and pressure, *i.e.* the cosmological constant Λ, can provide an acceleration of the expansion leading to an arbitrarily old universe. A universe with $\Omega_0 + \Omega_\Lambda = 1$ is special in that it is the only one that is spatially flat. Dynamical measurements of the mass in the halo of galaxies from their velocity dispersion implies that $\Omega_0 \gtrsim 0.1 - 0.3$. The inequality results from the fact that these measurements cannot probe the amount of mass that is not clustered with galaxies. Large scale velocity fields can test larger regions and though the situation to date is far from clear, current measurements tend to yield slightly higher values for Ω_0 (see *e.g.* [156] for a recent review).

Let us examine the constituents of the total density. Luminous matter in the form of stars in the central part of galaxies only accounts for $\Omega_* \simeq 0.004$ of the critical density. Compared with dynamical measurements, this indicates that most of the matter in the universe is dark. On the other hand, the CMB energy density $\Omega_\gamma h^2 = 2.38 \times 10^{-5} \Theta_{2.7}^4$,

where $\Theta_{2.7} = T_0/2.7\text{K}$. Although negligible today, in the early universe it increases in importance relative to the matter energy density ρ_m since $\rho_\gamma/\rho_m \propto 1+z$ due to the redshift. With the photon density thus fixed through the CMB temperature, primordial nucleosynthesis and observations of the light element abundances imply that the baryon fraction is low $\Omega_b h^2 = 0.01 - 0.02$ [151, 171]. A significant amount of non-baryonic dark matter is apparently present in the universe. The amount and nature of dark matter in the universe has significant consequences for structure formation. The most crucial aspect of its nature for these purposes is the mass of its constituent particles. Collisionless dark matter, unlike baryonic matter, does not suffer dissipative processes. Thus the particle mass determines whether their rms velocity is high enough to escape gravitational collapse.

CMB anisotropies can provide information on all these fundamental issues and more. Since the issue of anisotropy formation is of such central importance, its systematic development occupies the greater part of this work §4–7. Gravitational and Compton coupling of the CMB represent intertwining themes that recur throughout these chapters. It is therefore useful to give here a brief exposition of these concepts, their importance for anisotropy formation, and their implications for cosmology [85].

1.2 Anisotropy Formation

> *Words are for catching ideas; once you've caught the idea, you can forget about the words. Where can I find a man who knows how to forget about words so that I might have a few words with him?*
>
> *–Chuang-tzu, 26*

Fluctuations in the total matter density, which includes decoupled species such as the neutrinos and possibly collisionless dark matter, interact with the photons through the gravitational potentials they create. These same fluctuations grow by gravitational attraction, *i.e.* infall into their own potential wells, to eventually form large scale structure in the universe. Their presence in the early universe is also responsible for anisotropy formation.

Before redshift $z_* \simeq 1000$, the CMB was hot enough to ionize hydrogen. Compton scattering off electrons, which are in turn linked to the protons through Coulomb interactions, strongly couples the photons to the baryons and establishes a photon-baryon fluid. Photon pressure resists compression of the fluid by gravitational infall and sets up acoustic oscillations. At z_*, recombination produces neutral hydrogen and the photons last scat-

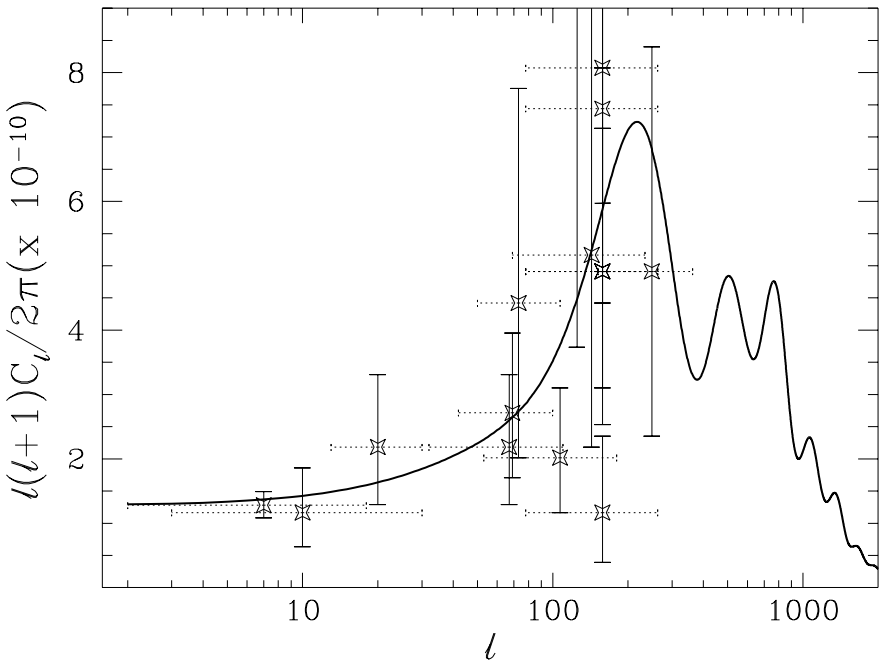

Figure 1.3: Anisotropies: Theory and Experiment

Anisotropy data of current CMB experiments from Tab. B.3 compiled by [146]. Dotted horizontal "error bars" are the half power angular range of the experiment. Overplotted is the predicted anisotropy power spectrum C_ℓ in a typical model: standard CDM with $\Omega_0 = 1$, $h = 0.5$, $\Omega_B = 0.05$, scale invariant scalar initial fluctuations, and arbitrary normalization. The corresponding angle on the sky is approximately $100/\ell$ degrees.

ter. Regions of compression and rarefaction at this epoch represent hot and cold spots respectively. Photons also suffer gravitational redshifts from climbing out of the potentials on the last scattering surface. The resultant fluctuations appear to the observer today as anisotropies on the sky. By developing the simple picture outlined above in greater detail, we show how realistic anisotropies such as those depicted in Fig 1.3 are formed.

Notation

Although sky maps such as Fig. 1.2 are visually impressive, the anisotropy must be analyzed statistically. For gaussian fluctuations, the statistical content is encapsulated in the two point temperature correlation function, or equivalently its angular decomposition into Legendre moments C_ℓ. In Fig. 1.3, we show a typical prediction for the anisotropy power spectrum C_ℓ compared with the current state of observations.

Predictions for C_ℓ are obtained by tracking the evolution of temperature fluctu-

ations. Their equations of motion take on a simple form when decomposed into normal modes. These are plane waves for a flat geometry, referred to in this chapter as such even when considering their open geometry generalization (see §4.1.1 and [71, 175]). We represent temperature fluctuations in Newtonian form, which simplifies concepts such as infall and redshift, by defining them on the spatial hypersurfaces of the conformal Newtonian gauge (see §4.3).

Under the gravitational force F, a temperature perturbation $\Theta_0 = \Delta T/T$ of comoving wavenumber k evolves almost as a simple harmonic oscillator before recombination [82] $(1+R)\ddot{\Theta}_0 + \frac{k^2}{3}\Theta_0 \simeq F$. The overdots represent derivatives with respect to conformal time $\eta = \int (1+z)dt$ with $c = 1$ and $R = 3\rho_b/4\rho_\gamma = 3.0 \times 10^4 (1+z)^{-1}\Omega_b h^2$ accounts for the baryonic contribution to the effective mass of the oscillator. Notice that the restoring force from photon pressure is independent of the baryon content. The frequency of the oscillator is constructed out of these quantities as $\omega = kc_s$ where the sound speed c_s, which measures the resistance of the fluid to compression, is $c_s \equiv \dot{p}/\dot{\rho} = 1/\sqrt{3(1+R)}$. The oscillator equation can thus be rewritten as $\ddot{\Theta}_0 + k^2 c_s^2 \Theta_0 \simeq F/(1+R)$.

Let us now consider the gravitational driving force $F/(1+R) \simeq -k^2\Psi/3 - \ddot{\Phi}$, where Ψ is the Newtonian gravitational potential, obtained from density fluctuations via the generalized Poisson equation, and $\Phi \simeq -\Psi$ is the perturbation to the space curvature. They also represent plane wave fluctuations in the time-time and space-space metric components respectively. The sign convention reflects the fact that overdensities create positive space curvature and negative potentials, *i.e.* potential wells. In real space though, a single plane wave represents both overdense *and* underdense regions. We use the former to guide intuition since the distinction is only in sign.

1.2.1 Acoustic Oscillations

Let us first consider temperature fluctuations before recombination in the case of a *static* potential [48, 15, 92]. Although only appropriate for a universe which has *always* been matter dominated, it illustrates the general nature of the acoustic oscillations. In this case, $F = -k^2(1+R)\Psi/3$ and represents the usual driving force of gravity that leads to infall into potential wells. Since big bang nucleosynthesis implies that the baryon density is low, $\Omega_b h^2 \simeq 0.01 - 0.02$, as a first approximation assume that $R \ll 1$ and the photons completely dominate the fluid $c_s \simeq 1/\sqrt{3}$.

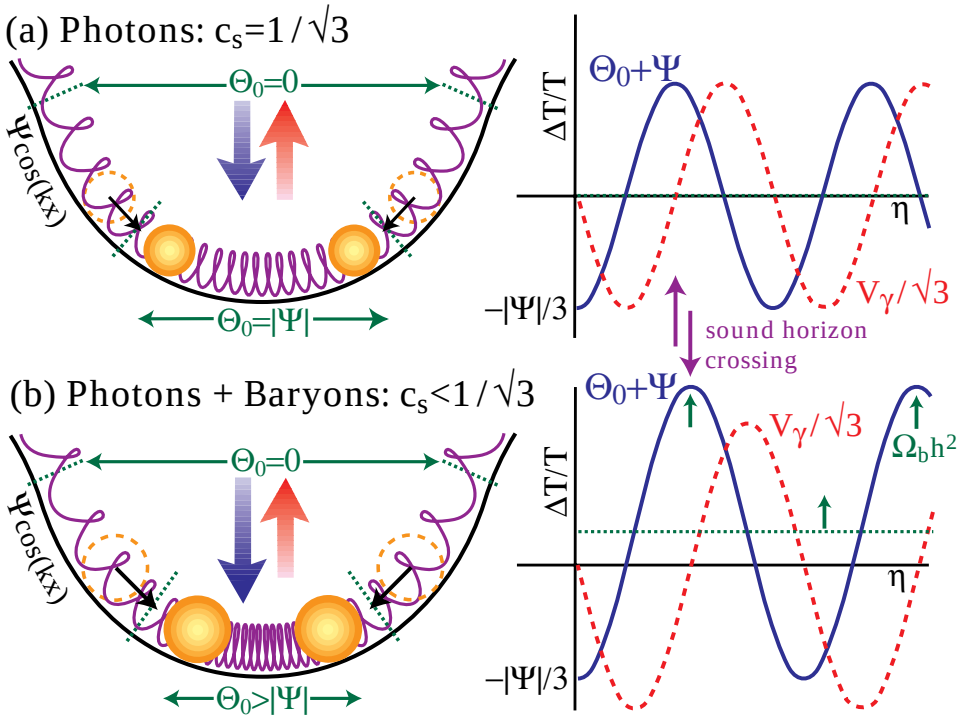

Figure 1.4: Acoustic Oscillations

(a) Photon-dominated system. Fluid compression through gravitational infall is resisted by photon pressure setting up acoustic oscillations. Displayed here is a potential well in real space $-\pi/2 \lesssim kx \lesssim \pi/2$. Gravity displaces the zero point so that at the bottom of the well, the temperature is $\Theta_0 = |\Psi| = -\Psi$ at equilibrium with $\Psi/3$ excursions. This displacement is exactly cancelled by the redshift Ψ a photon experiences climbing out from the bottom of the potential well. Velocity oscillations lead to a Doppler effect 90 degrees phase shifted from the temperature perturbation. (b) Photon-baryon system. Baryons increase the gravitating mass, causing more infall and a net zero point displacement, even after redshift. Temperature crests (compression) are enhanced over troughs (rarefaction) and velocity contributions.

Gravitational infall compresses the fluid until resistance from photon pressure reverses the motion. Since the gravitational force is constant in this case, it merely shifts the zero point of the oscillation to $\Theta_0 = -\Psi$. To determine the amplitude of the oscillations, we must first fix the initial conditions. The relation between the matter density fluctuations and the potential $\delta_m(0) = -2\Psi$ is fixed by demanding consistency with the Poisson and Euler equations. Let us assume adiabatic initial conditions for the photons $\Theta_0(0) = \frac{1}{3}\delta_m(0) = -\frac{2}{3}\Psi$ and $\dot{\Theta}_0(0) = 0$ (see Fig. 1.4a). In this case, the photons follow the matter, making the temperature higher inside a potential well. The effective initial displacement of $\Theta_0(0) + \Psi = \frac{1}{3}\Psi$ then evolves as $\Theta_0(\eta) = \frac{1}{3}\Psi\cos(kc_s\eta) - \Psi$. At last scattering η_*, the photons decouple from the baryons and stream out of potential wells suffering gravitational redshifts equal to Ψ. We thus call $\Theta_0 + \Psi$ the *effective* temperature fluctuation. Here the redshift exactly cancels the zero point displacement since gravitational infall and redshift are one and the same for a photon-dominated system.

The phase of the oscillation at last scattering determines the effective fluctuation. Since the oscillation frequency $\omega = kc_s$, the critical wavenumber $k = \pi/c_s\eta_*$ is essentially at the scale of the *sound horizon* $c_s\eta_*$ (see Fig 1.4). Larger wavelengths will not have evolved from the initial conditions and possess $\frac{1}{3}\Psi$ fluctuations after gravitational redshift. This combination of the intrinsic temperature fluctuation and the gravitational redshift is the well known Sachs-Wolfe effect [138]. Shorter wavelength fluctuations can be frozen at different phases of the oscillation. Since fluctuations as a function of k go as $\cos(kc_s\eta_*)$ at last scattering, there will be a harmonic series of temperature *fluctuation* peaks with $k_m = m\pi/c_s\eta_*$ for the mth peak. Odd peaks thus represent the compression phase (temperature crests), whereas even peaks represent the rarefaction phase (temperature troughs), inside the potential wells.

1.2.2 Baryon Drag

Though effectively pressureless, the baryons still contribute to the inertial and gravitational mass of the fluid $m_{\rm eff} = 1+R$. This changes the balance of pressure and gravity as baryons drag the photons into potential wells. As the baryon content R is increased, gravitational infall leads to greater compression of the fluid, *i.e.* a further displacement of the oscillation zero point (see Fig. 1.4b). Since the redshift is not affected by the baryon content, this relative shift remains after last scattering to enhance all peaks from compression over

those from rarefaction. If the baryon photon ratio R were constant, $\Theta(\eta) + \Psi = \frac{1}{3}\Psi(1 + 3R)\cos(kc_s\eta) - R\Psi$, with compressional peaks a factor of $(1 + 6R)$ over the $R = 0$ case. In reality, the effect is reduced since $R \to 0$ at early times.

Finally the *evolution* of the effective mass has a effect of its own. In classical mechanics, the ratio of energy $E = \frac{1}{2}m_{\rm eff}\omega^2 A^2$ to frequency of an oscillator ω is an adiabatic invariant. Thus for the slow changes in $\omega \propto (1 + R)^{-1/2}$, the amplitude of the oscillation varies as $A \propto (1 + R)^{-1/4}$. Since $R(\eta_*) = 30\Omega_b h^2 \lesssim 1$ at recombination, this is ordinarily not a strong effect.

1.2.3 Doppler Effect

Since the turning points are at the extrema, the fluid velocity oscillates 90 degrees out of phase with the density (see Fig. 1.4a). Its motion relative to the observer causes a Doppler shift. Whereas the observer velocity creates a pure dipole anisotropy on the sky, the fluid velocity causes a spatial temperature variation $V_\gamma/\sqrt{3}$ on the last scattering surface from its line of sight component. For a photon-dominated $c_s \simeq 1/\sqrt{3}$ fluid, the velocity contribution is equal in amplitude to the density effect [48, 92]. This photon-intrinsic Doppler shift should be distinguished from the scattering-induced Doppler shift of reionized scenarios (see §7.1.3 and [162]).

The addition of baryons significantly changes the relative velocity contribution. As the effective mass increases, conservation of energy requires that the velocity decreases for the same initial temperature displacement. Thus the *relative* amplitude of the velocity scales as c_s. In the toy model of a constant baryon-photon density ratio R, the oscillation becomes $V_\gamma/\sqrt{3} = \frac{1}{3}\Psi(1 + 3R)(1 + R)^{-1/2}\sin(kc_s\eta)$. Notice that velocity oscillations are symmetric around zero leading to even more prominent compressional peaks (see Fig. 1.4b). Even in a universe with $\Omega_b h^2$ given by nucleosynthesis, R is sufficiently large to make velocity contributions subdominant.

1.2.4 Potential Evolution

All realistic models involve potentials which are time-dependent, leading to a non-trivial gravitational driving force that can greatly enhance the prominence of the acoustic peaks [82, 83]. We have hitherto assumed that matter dominates the energy density. In reality, radiation dominates above the redshift of equality $z_{eq} = 2.4 \times 10^4 \Omega_0 h^2$, assuming

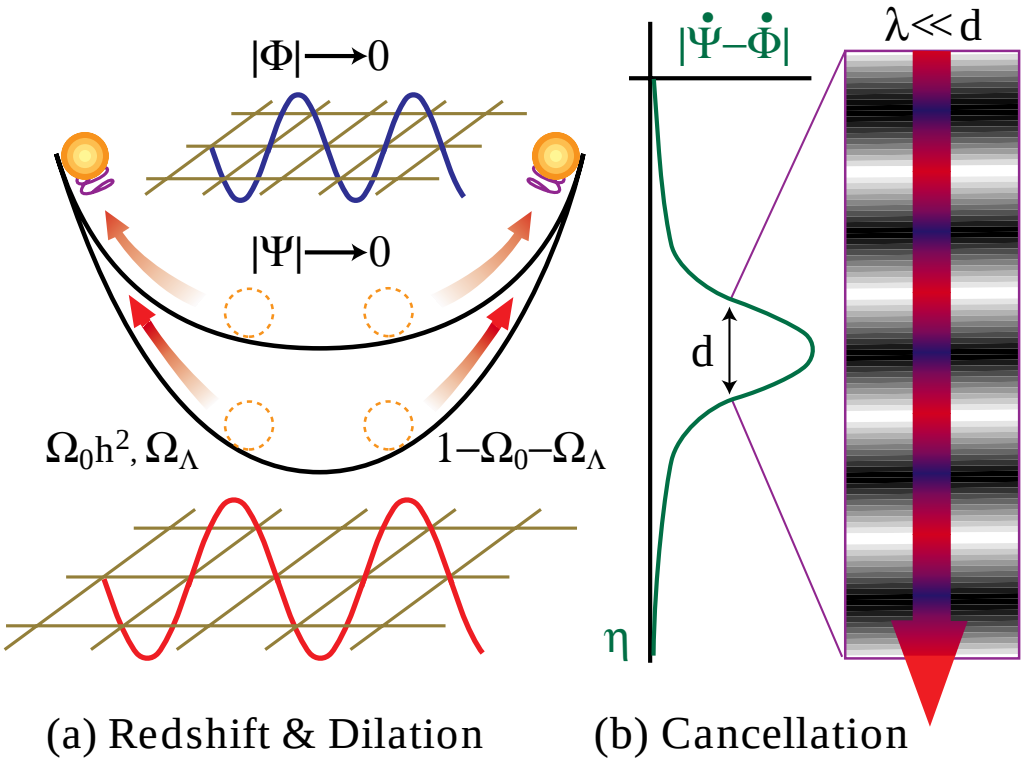

Figure 1.5: Differential Redshift and Dilation

Gravitational redshift and dilation effects in a time dependent potential. Time variability occurs whenever the matter is not the sole dynamical factor and thus probes $\Omega_0 h^2$, Ω_Λ, $1-\Omega_0-\Omega_\Lambda$ and any isocurvature perturbations. (a) Decay of the potential $|\Psi|$ decreases the gravitational redshift leading to an effective blueshift in the well. The implied curvature perturbation $|\Phi|$ decay represents a "contraction of space" which blueshifts photons through time dilation, nearly doubling the Ψ effect. (b) In the free streaming limit after last scattering, these two mechanisms combine to form the ISW effect. Redshift-blueshift cancellation cuts off contributions at small scales where the photon traverses many wavelengths during the decay.

the usual three flavors of massless neutrinos. The feedback from radiation perturbations into the gravitational potential makes the CMB sensitive to the matter-radiation ratio in the background *and* the fluctuations.

Consider first adiabatic initial conditions as before. Inside the sound horizon, radiation pressure prevents gravitational infall during radiation domination. Energy density fluctuations consequently can no longer maintain a constant gravitational potential. Counterintuitively, this decaying potential can actually enhance temperature fluctuations through its near resonant driving force. Since the potential decays after sound horizon crossing, it mimics $\cos(kc_s\eta)$ for $kc_s\eta \lesssim \pi$. Consequently, it drives the first compression without a counterbalancing effect on the subsequent rarefaction or gravitational redshift.

Moreover, there is another effect. Recall that the space curvature perturbation follows the potential as $\Phi \simeq -\Psi$. Since the forcing function $F/(1+R) \simeq -\ddot{\Phi} - k^2\Psi/3$, a changing Φ also drives oscillations. As Φ is a perturbation to the spatial metric, its change induces a time-dilation effect which is wholly analogous to the cosmological redshift due to the expansion. Heuristically, the overdensities which establish the potential well "stretch" the space-time fabric (see Fig. 1.5a). As the potential well decays, it re-contracts. Photons which are caught in this contraction find their wavelength similarly contracted, *i.e.* blueshifted. Thus a differential change in Φ leads to a dilation effect, $\dot{\Theta}_0 = -\dot{\Phi}$, and consequently a forcing effect on $\ddot{\Theta}_0$ of $-\ddot{\Phi}$ as required.

If Ψ were exactly $\cos(kc_s\eta)$, then $\ddot{\Phi}$ would double the driving force. Detailed calculation shows that the oscillation amplitude is boosted to $\simeq 5$ times the Sachs-Wolfe effect of $\frac{1}{3}\Psi$ (see §5.2.2). Only short wavelengths, which cross the sound horizon during the radiation-dominated epoch, experience this enhancement. For $\Omega_0 h^2 \simeq 0.25$, the sound horizon at equality is several times smaller than that at last scattering. Hence delaying equality, by lowering $\Omega_0 h^2$ or increasing the number of relativistic species, boosts the amplitude of oscillations for the first few peaks. Finally, the decay of the potential Ψ also removes the zero point shift and thus lifts the pattern of alternating heights for the peaks.

As a second example of forced oscillations, consider isocurvature perturbations. In this case, the matter alone carries the initial fluctuations, *i.e.* $\Theta_0(0) = 0$ and since the radiation dominates the energy density, $\Phi(0) = 0 = \Psi(0)$ as well. However $\dot{\Theta}(0) \neq 0$ and is set to counteract the gravitational attraction of the matter. Consequently, the potential grows to be significant only near sound horizon crossing and subsequently decreases if the universe is radiation dominated. The forcing function resembles $\sin(kc_s\eta)$ and thus drives

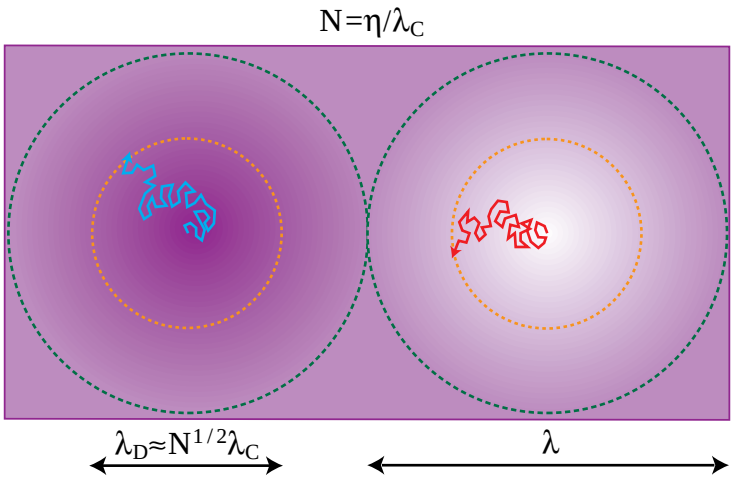

Figure 1.6: Photon Diffusion

Photon diffusion mixes hot photons from overdense regions and cold photons from underdense regions as the diffusion length λ_D exceeds the wavelength λ. Scattering averages the two and rapidly damps anisotropies. The diffusion length is given by a random walk of stepsize the Compton mean free path λ_C. The number of steps the photon traverses in the age of the universe η is η/λ_C. Thus the diffusion length scales as $\lambda_D \simeq N^{1/2}\lambda_C = (\eta\lambda_C)^{1/2}$. The Compton mean free path increases near recombination causing extensive damping at last scattering.

the sine harmonic of oscillations. Furthermore, since fluctuations are initially established to counter gravity, infall enhances *even* rather than odd peaks. Outside the sound horizon, dilation implies that $\Theta_0(\eta_*) = -\Phi(\eta_*)$, creating a Sachs-Wolfe effect of $[\Theta_0 + \Psi](\eta_*) \simeq 2\Psi(\eta_*)$.

1.2.5 Photon Diffusion Damping

In reality, the photons and baryons are not perfectly coupled since the photons possess a mean free path in the baryons λ_C due to Compton scattering. As the photons random walk through the baryons, hot spots and cold spots are mixed (see Fig. 1.6). Fluctuations thereafter remain only in the unscattered fraction causing a near exponential decrease in amplitude as the diffusion length $\lambda_D \sim \sqrt{N}\lambda_C = \sqrt{\eta\lambda_C}$ overtakes the wavelength [150].

At last scattering, the ionization fraction x_e decreases due to recombination, thus increasing the mean free path of the photons $\lambda_C \propto (x_e n_b)^{-1}$. The effective diffusion scale is therefore extremely sensitive to the ionization history in addition to the baryon number density n_b. Subtle effects during and even before last scattering can have a measurable effect

on the damping [93, 77]. Moreover, if last scattering is delayed, *e.g.* by early reionization, diffusion continues and can destroy all the acoustic peaks (see §7.1). Assuming a standard recombination ionization history however, the approximate scaling can be obtained from the Saha equation for the ionization at fixed redshift or temperature, $x_e \propto (\Omega_b h^2)^{-1/2}$. The final damping length therefore approximately scales as $\lambda_D(\eta_*) \propto \eta_*^{1/2}(\Omega_b h^2)^{-1/4}$. For high $\Omega_b h^2$ models, this scaling must be modified due to the high Lyman-α opacity at recombination [84].

1.2.6 Integrated Sachs-Wolfe Effect

After last scattering, the photons free stream toward the observer. Only gravitational effects can further alter the temperature. The differential redshift from $\dot{\Psi}$ and dilation from $\dot{\Phi}$ discussed above must be integrated along the trajectory of the photons. We thus call the combination the *integrated* Sachs-Wolfe (ISW) effect [138]. For adiabatic models, it can contribute via the potential decay for modes that cross the sound horizon between last scattering and full matter domination. In isocurvature models, potential *growth* outside the sound horizon makes the ISW effect dominate over the Sachs-Wolfe effect for all wavelengths larger than the sound horizon at η_* (see §6.2.6). Because these effects are sensitive to the radiation content and occur primarily at early times, we call them *early* ISW effects. In an open or Λ model, the universe enters a rapid expansion phase once matter no longer dominates the expansion. We call the effect of the resultant potential decay the *late* ISW effect.

One additional subtlety is introduced in ISW effects. If the potential decays while the photon is in an underdense region, it will suffer an effective redshift rather than a blueshift. Contributions from overdense and underdense regions will cancel and damp the ISW effect if the decay time is much greater than the light travel time across a wavelength (see Fig. 1.5). The damping does not occur for the *early* ISW effect. Since it arises when the perturbations are outside or just crossing the horizon, the time scale for the decay is always less than, or comparable to, the light travel time across a wavelength. For the late ISW effect, decay takes on the order of an expansion time at curvature or Λ domination independent of the wavelength. Thus, cancellation leads to a gradual damping in k of contributions as the wavelength becomes smaller than the horizon at the decay epoch. For a fixed Ω_0, the decay epoch occurs much later in flat $\Omega_\Lambda + \Omega_0 = 1$ models than open ones.

Consequently, Λ models will suffer cancellation of late ISW contributions at a much larger scale than open models [98]. In summary, the epoch that the universe exits the radiation ($\Omega_0 h^2$) and matter-dominated phase ($\Omega_\Lambda, 1-\Omega_0-\Omega_\Lambda$) is imprinted on the CMB by the early and late ISW effects respectively.

1.2.7 Projection Effects

We have been considering the generation of temperature fluctuations in space. However, what one actually observes are temperature anisotropies on the sky. The connection between the two is that a spatial fluctuation on a distant surface, say at last scattering for the acoustic effects, appears as an anisotropy on the sky. Three quantities go into this conversion: the spectrum of spatial fluctuations, the distance to the surface of their generation, and curvature or lensing in light propagation to the observer (see Fig. 1.7).

For the acoustic contributions, the k modes that reach extrema in their oscillation at last scattering form a harmonic series of peaks related to the sound horizon. This in turn is approximately $\eta_*/\{1+C[1+R(\eta_*)]^{1/2}\}$, where $R(\eta_*)=30\Omega_b h^2$ and $C\simeq\sqrt{3}-1$. Since $\Omega_b h^2$ must be low to satisfy nucleosynthesis constraints, the sound horizon will scale roughly as the particle horizon η_*. The particle horizon at last scattering itself scales as $\eta_*\propto(\Omega_0 h^2)^{-1/2} f_R$. Here $f_R=[1+(24\Omega_0 h^2)^{-1}]^{1/2}-(24\Omega_0 h^2)^{-1/2}$ and is near unity if the universe is matter dominated at η_*. For low $\Omega_0 h^2$, radiation allows for more rapid early expansion and consequently a smaller horizon scale. In a flat Λ universe, the distance to the last scattering surface scales approximately as $\eta_0\propto(\Omega_0 h^2)^{-1/2} f_\Lambda$ with $f_\Lambda = 1+0.085\ln\Omega_0$. Notice that the two behave similarly at high $\Omega_0 h^2$. Since the acoustic angle $\theta_A\propto\eta_*/\eta_0$, the leading term $(\Omega_0 h^2)^{-1/2}$ has no effect. Slowly varying corrections from f_R/f_Λ decreases the angular scale somewhat as $\Omega_0 h^2$ is lowered. On the other hand, the damping scale subtends an angle $\theta_D\simeq\lambda_D/\eta_0\propto(\Omega_0 h^2)^{1/4}(\Omega_b h^2)^{-1/4} f_R^{1/2}/f_\Lambda$. Even in a low $\Omega_0 h^2$ universe θ_D is only weakly dependent on h unlike θ_A the acoustic scale.

By far the most dramatic effect is due to *background* curvature in the universe [158]. If the universe is open, photons curve on their geodesics such that a given scale subtends a much smaller angle in the sky than in a flat universe. In a $\Lambda=0$ universe, the angle-distance relation yields $\theta_A\propto\eta_*\Omega_0 h$, *i.e.* $\propto\Omega_0^{1/2} f_R$. Likewise, the damping scale subtends an angle $\theta_D\propto\lambda_D\Omega_0 h$, *i.e.* $\propto\Omega_0^{3/4}\Omega_b^{-1/4} f_R^{1/2}$. At *asymptotically* high and low $\Omega_0 h^2$, $f_R\simeq 1$ and $f_R\propto(\Omega_0 h^2)^{1/2}$ respectively, so that there is a weak but different scaling

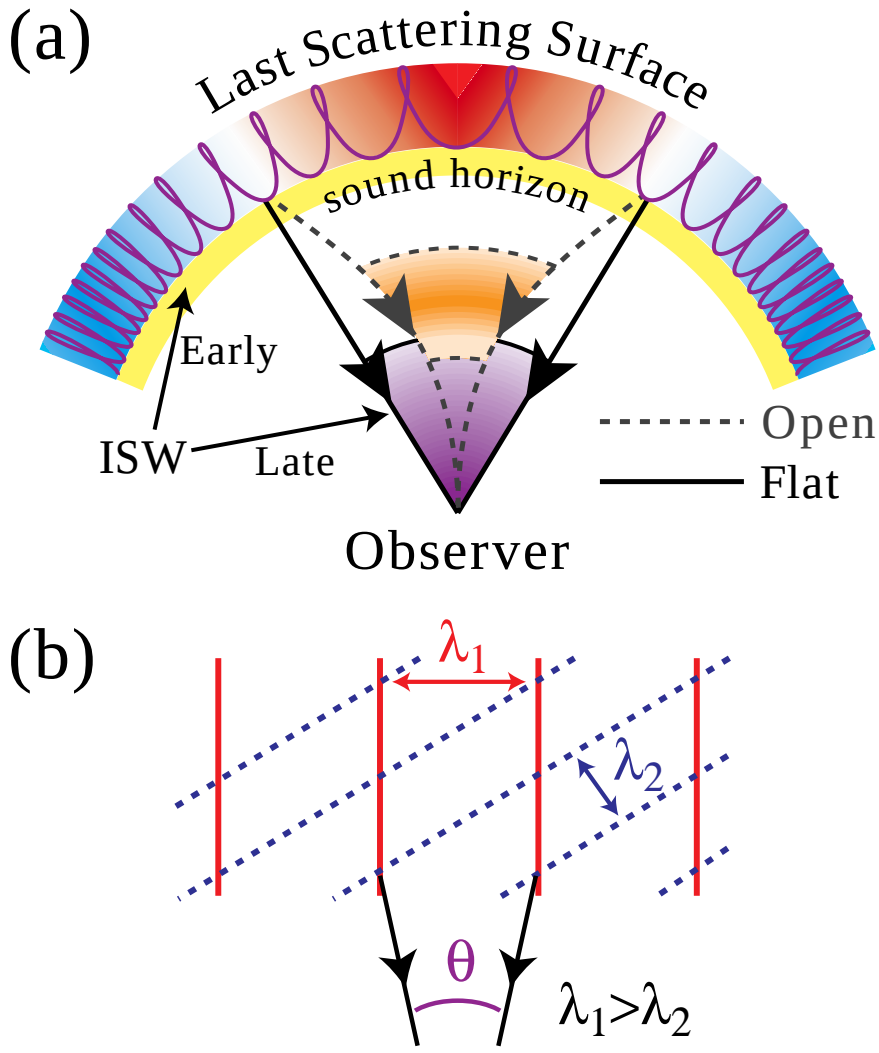

Figure 1.7: Projection Effect

(a) Acoustic contributions exhibit a series of peaks with decreasing angle beginning at the angular scale the sound horizon subtends at last scattering. This scale decreases significantly as the curvature increases due to geodesic deviation. Contributions after last scattering, come from a smaller physical scale for the same angular scale, which pushes the late ISW effect of flat Λ and open models to larger angles. (b) The orientation of the plane wave projected on the surface of last scattering leads to aliasing of power from shorter wavelengths onto larger angles. This smooths out sharp features and prevents a steeply rising (blue) anisotropy spectrum.

with h and strong but similar scaling with Ω_0 for the two angles. The latter should be an easily measurable effect [96].

Contributions from after last scattering, such as the ISW effects, arise from a distance closer to us. A given scale thus subtends a larger angle on the sky (see Fig. 1.7). Their later formation also implies that the radiation correction factor f_R will be smaller. For example, the angle subtended by the adiabatic early ISW effect scales nearly as $\Omega_0^{1/2}$ in a $\Lambda = 0$ universe even at low $\Omega_0 h^2$.

The above discussion implicitly assumes an one-to-one correspondence of linear scale onto angle that is strictly only true if the wavevector is perpendicular to the line of sight. In reality, the orientation of the wavevector leads to aliasing of different, in fact larger, angles for a given wavelength (see Fig. 1.7b). This is particularly important for Doppler contributions which vanish for the perpendicular mode (see §7.1.4). Moreover if there is a lack of long wavelength power, *e.g.* in typical baryon isocurvature models, large angle anisotropies are dominated by aliasing of power from short wavelengths. Consequently, the angular power spectrum may be less blue than the spatial power spectrum (see §6.2.6). On the other hand, for so called "scale invariant" or equal weighting of k modes, aliasing tends to smear out sharp features but does not change the general structure of the real to angular space mapping. It is evident that gravitational lensing from the curvature *fluctuations* of overdense and underdense regions has a similar but usually smaller effect [148].

1.3 Anisotropy Spectrum

Anisotropy formation is a simple process that is governed by gravitational effects on the photon-baryon fluid and the photons alone before and after last scattering respectively. The component contributions contain detailed information on classical cosmological parameters. Let us now put them together to form the total anisotropy spectrum.

The popular scale invariant adiabatic models provide a useful example of how cosmological information is encoded into the anisotropy spectrum. Specifically by scale invariant, we mean that the logarithmic contribution to the gravitational potential is initially constant in k. For open universes, this is only one of several reasonable choices near the curvature scale [95, 110, 134, 20]. In Fig. 1.8, we display a schematic representation of the anisotropy spectrum which separates the various effects discussed above and identifies their dependence on the background cosmology.

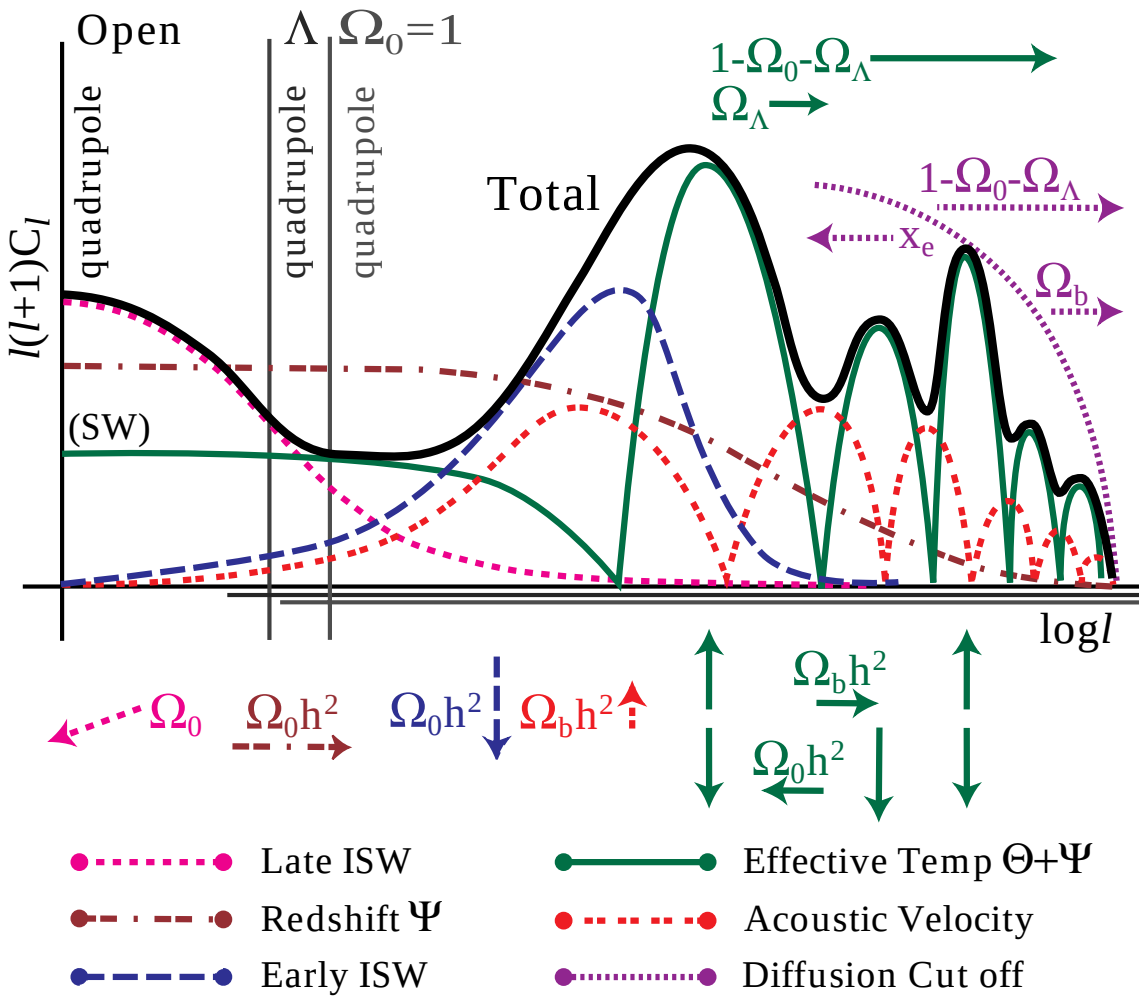

Figure 1.8: Total Anisotropy Spectrum

A schematic representation for scale invariant adiabatic scalar models. Features in open models are shifted to significantly smaller angles compared with Λ and $\Omega_0 = 1$ models, represented here as a shift in the ℓ axis beginning at the quadrupole $\ell = 2$. The monopole and dipole fluctuations are unobservable due to the mean temperature and peculiar velocity at the point of observation. The effective temperature at last scattering $[\Theta+\Psi](\eta_*)$ includes the gravitational redshift effect $\Psi(\eta_*)$. At large scales, the effective temperature goes to $\Psi(\eta_*)/3$ and is called the Sachs-Wolfe (SW) contribution. In reality, small scale acoustic contributions from the effective temperature and velocity are smoothed out somewhat in ℓ due to projection effects (see Fig. 1.7).

Changing the overall dynamics from $\Omega_0 = 1$ through flat Λ models to open models is similar to shifting the spectrum in angular space toward smaller angles. Beginning at the largest angles, the ISW effect from late potential decay dominates in $\Omega_0 \ll 1$ models. Cancellation suppresses contributions for wavelengths smaller than the particle horizon at the exit from matter domination. This damping extends to larger angles in Λ than in open models affecting even the quadrupole. At scales much larger than the sound horizon at η_* and particle horizon at equality, the effective temperature, or Sachs-Wolfe effect, is $[\Theta + \Psi](\eta_*) \simeq \frac{1}{3}\Psi(\eta_*)$. Shifting equality through $\Omega_0 h^2$ changes the redshift contribution $\Psi(\eta_*)$. For scales just above the sound horizon, the early ISW effect boosts fluctuations as the relative radiation content is increased by lowering $\Omega_0 h^2$. In sufficiently low Ω_0 open models, the late and early ISW effects merge and entirely dominate over the last scattering surface effects at large angles.

The first of a series of peaks from the acoustic oscillations appear on the sound horizon at η_*. In the total spectrum, the first acoustic peak merges with the early ISW effect. A lower $\Omega_0 h^2$ thus serves to broaden out and change the angular scaling of this combined feature. The acoustic peak heights also depend strongly on $\Omega_0 h^2$ for the first few peaks due to the driving effects of infall and dilation. Furthermore, greater infall due to the baryons allows more gravitational zero point shifting if $\Omega_0 h^2$ is sufficiently high to maintain the potentials. Odd peaks will thus be enhanced over the even, as well as velocity contributions, with increasing $\Omega_b h^2$. The location of the peaks is dependent on the sound horizon, distance to last scattering, and the curvature. In a low $\Omega_b h^2$, high $\Omega_0 h^2$ universe, it is sensitive only to the curvature $1 - \Omega_0 - \Omega_\Lambda$. Finally, the physics of recombination sets the diffusion damping scale which cuts off the series of acoustic peaks.

1.4 Robustness to Initial Conditions

How robust are anisotropies to model changes? Obviously, changing the initial spectrum will significantly modify the spectrum. For example, isocurvature conditions and tilt can alter the relative contributions of the various effects. The lack of super-curvature modes in open inflationary models can also suppress the low order multipoles [111]. On the other hand, they may be boosted by gravitational wave ISW contributions [168, 37].

Acoustic oscillations however are unavoidable, if there are potential perturbations before last scattering. Even exotic models such as defect-induced fluctuations should give

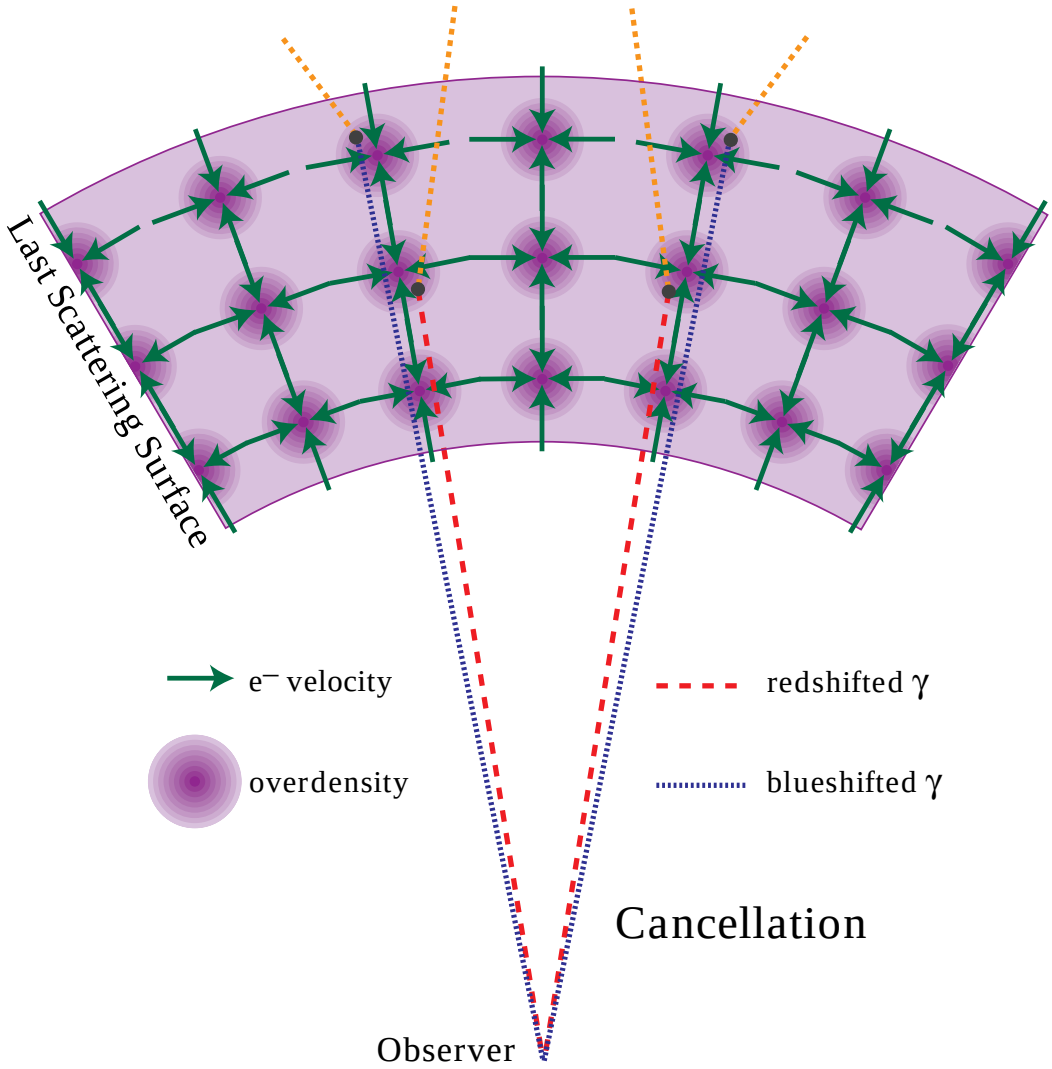

Figure 1.9: Cancellation Mechanism

If the coherence scale, *i.e.* wavelength, of the perturbation is under the thickness of the last scattering surface, the photons suffer alternating Doppler shifts depending on whether the photon last scattered in the fore or rear of the perturbation. The small scale Doppler effect is therefore severely cancelled.

rise to acoustic contributions of some form. Since adiabatic and isocurvature conditions drive two different harmonics, they can be distinguished by the relation between the peaks and the sound horizon at last scattering [83]. The *locations* of the peaks are then dependent only on the background cosmology, *i.e.* mainly on the curvature but also on a combination of $\Omega_b h^2$, Ω_Λ and $\Omega_0 h^2$. On the other hand, the difference in heights between odd and even peaks is a reasonably robust probe of the baryon-photon ratio, *i.e.* $\Omega_b h^2$, relative to the matter-radiation ratio at last scattering, *i.e.* $\Omega_0 h^2$ and possibly even the number of massless neutrinos. Finally, the damping scale probes the baryon content and the detailed physics of recombination. If acoustic oscillations are detected in the anisotropy data, clearly we will be able to measure many parameters of classical cosmology.

1.5 Reionization

The one caveat to these considerations is that reionization can completely erase the acoustic oscillations. In a model with sufficiently early reionization, *i.e.* $z_i \gg 10$, the photon diffusion length grows to be the horizon scale at the new last scattering surface and consequently damps all of the peaks. In models such as CDM, structure forms late and early reionization is highly unlikely. However, it is worthwhile to consider its general effects on the CMB in the event that structure formation proceeded by a qualitatively different route.

CMB fluctuations can be regenerated once the baryons are released from Compton drag to evolve independently $z_d = 160(\Omega_0 h^2)^{1/5} x_e^{-2/5}$ (see §7.1.3). Baryonic infall into potential wells leads to electron bulk velocities which induce Doppler shifts in the scattered photons. If the universe remains ionized, last scattering effectively occurs when the Compton scattering time exceeds the expansion time. Thus the thickness of the last scattering surface is on the order of the horizon size at last scattering. At small scales, this thickness spans many wavelengths of the perturbation. Photons that last scatter from the fore and rear of the perturbation encounter electrons with oppositely directed infall velocities (see Fig. 1.9). Just like the late ISW effect, the net contribution will be cancelled at small scales.

Cancellation is particularly severe for the linear theory Doppler effect (see §7.1.4). This implies that higher order terms in perturbation theory will dominate the anisotropy at small scales. As we show in §7.2, the dominant second order effect is due to a coupling of density and velocity perturbations called the Vishniac effect [121, 169]. It arises since the

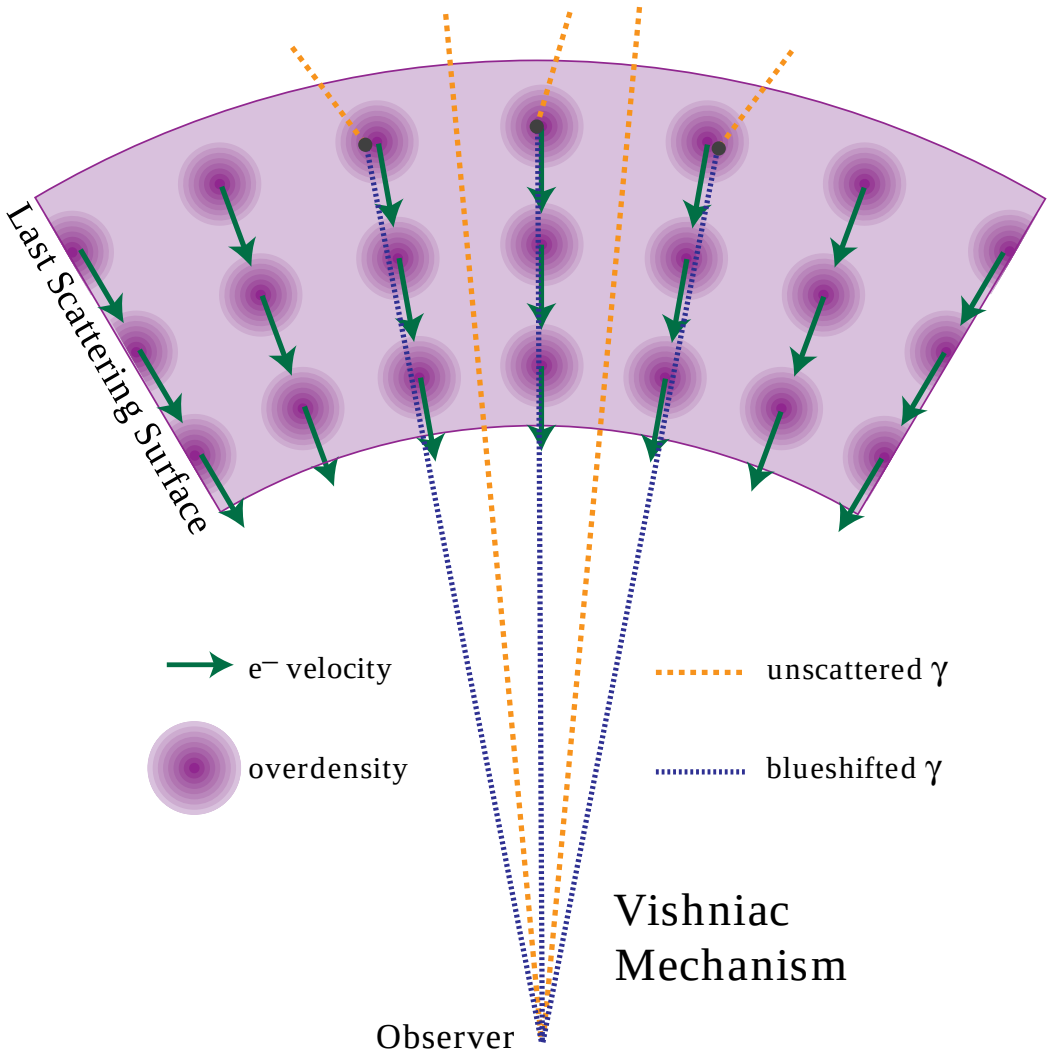

Figure 1.10: Vishniac Mechanism

In an overdense region, the free electron density is higher. This increases the probability of scattering. If these overdense regions are also caught in a large scale bulk flow, this can lead to a small scale variation in the temperature through preferential scattering. The Vishniac mechanism thus relies on a coupling of large and small scale perturbation modes.

probability of a photon scattering off an overdensity is higher due to the increased electron density. If the overdense regions are also caught in a larger scale bulk flow, this can yield an anisotropy on the scale of the overdensity since a greater fraction of the photons suffer Doppler kicks along lines of sight that intersect overdensities (see Fig. 1.10). Since the effect depends on a coupling of modes, it is extremely sensitive to the shape and amplitude of the baryon power spectrum. Furthermore, the horizon size at last scattering is imprinted as the cancelled scale of the first order effect. Thus in the case of early reionization, the CMB can be used as a sensitive probe of the model for structure formation and the ionization history of the universe, but yields little model-independent information on the classical cosmological parameters. These secondary anisotropies are thus complementary to the primary ones. It is possible that the observed spectrum will contain an admixture of the two if reionization occurs but is not sufficiently early.